Chemical Engineering Journal 476 (2023) 146679

Contents lists available at ScienceDirect

Chemical Engineering Journal

journal homepage: www.elsevier.com/locate/cej

Combinatorial wound dressings loaded with synergistic antibiotics in the treatment of chronic infected wounds

Laura Miranda-Calderon [a,b,1], Cristina Yus [a,b,c,1], Cristina Remirez de Ganuza [a,b,c], Monica Paesa [a,b,c], Guillermo Landa [a,b,c,*], Elena Tapia [d], Estela Pérez [e,f], Marta Perez [f,g], Victor Sebastian [a,b,c,h], Silvia Irusta [a,b,c,h], Gracia Mendoza [c,h,*], Manuel Arruebo [a,b,c,h]

[a] Instituto de Nanociencia y Materiales de Aragón (INMA), CSIC-Universidad de Zaragoza, 50009 Zaragoza, Spain
[b] Department of Chemical and Environmental Engineering. University of Zaragoza, Campus Río Ebro-Edificio I+D, C/ Poeta Mariano Esquillor S/N, 50018 Zaragoza, Spain
[c] Aragon Health Research Institute (IIS Aragon), 50009 Zaragoza, Spain
[d] Animal Unit, University of Zaragoza, 50009 Zaragoza, Spain
[e] Department of Animal Pathology, University of Zaragoza, 177 Miguel Servet Street, 50013 Zaragoza, Spain
[f] Instituto Universitario de Investigación Mixto Agroalimentario de Aragón (IA2), University of Zaragoza, 50013 Zaragoza, Spain
[g] Department of Anatomy, Embriology and Animal Genetics, University of Zaragoza, 177 Miguel Servet Street, 50013 Zaragoza, Spain
[h] Networking Research Center on Bioengineering, Biomaterials and Nanomedicine, CIBER-BBN, 28029 Madrid, Spain

ARTICLE INFO

Keywords:
Wound dressing
Eudragit®
Electrospinning
Antibiotics
Chronic wound
Staphylococcus aureus

ABSTRACT

Advanced medicated wound dressings fabricated by electrospinning and electrospraying were prepared for the eradication of topical bacterial infections potentially applied in the management of infected acute and chronic non-healing wounds. Two different antibiotics (ciprofloxacin and rifampicin), with different aqueous solubilities and different mechanisms of antimicrobial action, were loaded within electrosprayed polymer microparticles and within electrospun nanofibers, respectively, to provide the resulting wound dressing with dually controlled antibiotic release kinetics. Due to the large surface area per volume ratio of the electrosprayed microparticles containing ciprofloxacin, an initial burst release was obtained. Simultaneously, the reduced surface area per volume ratio for the electrospun nanofibers together with the reduced aqueous solubility of rifampicin produced an extended rifampicin release over time. More importantly, a synergistic antimicrobial effect against Gram-positive and Gram-negative bacteria was observed when both antibiotics were combined. Biofilm formation prevention and the elimination of already formed mature bacterial biofilms were also successfully achieved using our advanced dressings. The lack of cytotoxicity of the advanced wound dressings here reported against eukaryotic cells at antimicrobial doses was also demonstrated using three different mammalian cell lines. Moreover, the advanced wound dressings successfully eliminated a *Staphylococcus aureus* mediated experimental infection in a chronic wound murine model showing their efficacy for the treatment of these complicated non-healing wounds. The strategy of advanced medicated wound dressings developed here may be used as a potential methodology for the fabrication of functional combinatorial materials that offer the ability to eradicate bacterial infections.

1. Introduction

Microbial infections seriously prevent or delay the conventional physiological healing processes after wounding [1]. Various substances released by pathogenic bacteria may cause an excessive and prolonged inflammatory response in the host tissues soon after colonization and infection, and they can seriously impair the wound healing process [2]. *Staphylococcus aureus*, among others, commonly forms biofilms which consist of coherent clusters of bacterial cells embedded in an extracellular polymeric matrix. This sessile situation offers the pathogen excellent protection from the host immunological activity and from antibiotic/antiseptic therapy. Due to the polymicrobial nature of

* Corresponding authors at: Aragon Health Research Institute (IIS Aragon), 50009 Zaragoza, Spain.
E-mail addresses: glanda@unizar.es (G. Landa), gmendoza@iisaragon.es (G. Mendoza).
[1] Both authors contributed equally to this work.

https://doi.org/10.1016/j.cej.2023.146679
Received 6 July 2023; Received in revised form 10 October 2023; Accepted 12 October 2023
Available online 14 October 2023

infected wounds, conventional treatment includes wound debridement, cleansing and antiseptic application [3].

All wounds, from the time of the skin incision, become colonized with bacteria from the air, surrounding skin, and from any contaminated material involved in the initial wounding [4]. Unless they appear infected, most uncomplicated wounds heal without the need of antibiotic therapy, but, in some cases, local antibiotic (e.g., mupirocin, nadifloxacin, neomycin, bacitracin, fusidic acid, etc.) treatment may be indicated on infected wounds as a second-line option when infection persists, but always taking into account that it is necessary to prevent by any means antimicrobial resistance development and hypersensitivity reactions [5]. However, topical antibiotics were proven to be effective in reducing the risk of infections in uncomplicated wounds compared to placebo or antiseptics [6]. Moreover, the use of antibiotics has resulted in many successful and improved clinical outcomes by reducing infections in surgical sites and in chronic open wound infections [7].

Rifampicin (RIF), a hydrophobic semisynthetic antibiotic, is commonly used in the treatment of a large variety of bacterial infections, including those mediated by Mycobacterium spp., Gram-positive cocci (*Staphylococci* and *Streptococci*), and certain Gram-negative pathogens [8]. RIF is always used in combination with other antibiotics to treat *S. aureus*-associate bacterial infections due to its high susceptibility to develop resistance. On the other hand, ciprofloxacin (CIP) is a fluoroquinolone derivative that acts as an antibacterial agent inhibiting the growth of both Gram-positive and Gram-negative bacteria. It has been reported that its use on infected topical wounds improves wound healing [9]. The synergy between CIP and RIF was previously observed against *S. aureus* isolates [10]. Moreover, Coe et al. [11] have shown that CIP combined with RIF gives bacteriostatic additive effect *in vitro* on two experimental strains of *S. aureus*, 69,898 and 6,989R. The combination of these two antibiotics was also successfully used in the treatment of early postoperative recurrent *Staphylococcus epidermidis* implant-associated infections [12]. Therefore, combination therapy is a successful approach to reduce antibiotic resistance but it is important to be aware of the fact that its application is strain specific, and additive, synergetic or even antagonistic effects have been reported.

When using antibiotic loaded wound dressings, an initial burst release would eradicate any commensal or exogenous bacteria present in the wound and a subsequent sustained release would avoid any further reinfection improving the clinical outcome [13]. Antimicrobial-loaded electrospun membranes having specific dual antimicrobial release kinetics could simultaneously aid in the elimination of the initial bioburden present after wounding and also in the subsequent prophylaxis facilitating the wound-healing regenerative process. Some examples in the recent literature describe the use of drug dual-carrier systems containing one antimicrobial (e.g., amoxicillin sodium) with different release kinetics for the development of controlled release dressings [14]. Electrospun core–shell polycaprolactone/gelatin nanofibers loading two antibacterial agents, a synthetic antibiotic (minocycline) and a natural extract (*Gymnema sylvestre*), were proposed as wound dressing. In this case, a potent antibacterial activity against commensal biofilm-forming pathogens, such as methicillin-resistant *S. aureus* (MRSA) and pathogenic *Pseudomonas aeruginosa,* was observed [15]. Moreover, previous studies have also revealed the efficiency of the combination of antibiotics loaded into electrospun nanofibers. Gentamicin sulfate (GS) and CIP were loaded into electrospun gelatin fibers achieving a significant decrease in the bacterial load in an *in vivo* murine model of a deep burn infected with *P. aeruginosa* [16]. The fabrication of a electrospun chitosan/poly(vinyl alcohol) scaffold containing different concentrations of colistin and meropenem exerted synergistic bactericidal action against extensively drug resistant (XDR) bacterial clinical isolates of *Acinetobacter baumannii* together with good biocompatibility, both *in vitro* and *in vivo* [17].

Fiber-based wound dressings offering sustained amoxicillin delivery have been also reported to promote wound healing [18]. On the other hand, particles provide a fast drug release due to their high surface to volume ratio. The use of two different morphologies, fibers for the loading of RIF and particles for the loading of CIP, in the same wound dressing, would provide a desired antibiotics release thanks to a fast-initial diffusion and a subsequent polymeric matrix erosion. Herein, we report an advanced wound dressing fabricated by electrospinning/electrospraying exhibiting high RIF and CIP loadings and antimicrobial synergy against *S. aureus* and *E. coli* cultures. RIF loaded Eudragit® RS100-based fibers were decorated with CIP loaded Eudragit® RS100-based microparticles both prepared by electrohydrodynamic techniques. Eudragit® RS100 is a cationic, pH independent non-biodegradable copolymer of methyl methacrylate, ethyl acrylate, and methacrylic acid ester with quaternary ammonium groups [19]. Under physiological pH, Eudragit® RS100 erodes and releases its contained cargo. The bactericidal activity of the as-prepared advanced dressings was tested *in vitro* against planktonic and biofilm-forming *E. coli* and *S. aureus* and their lack of cytotoxicity at the doses tested was analyzed on three model human cell lines (keratinocytes, macrophages and fibroblasts). Moreover, its efficacy in a chronic infection murine model was also evaluated and the histopathological examination demonstrated that the physiology of the skin was restored.

2. Material and methods

2.1. Materials

Eudragit® RS100 (RS100) was purchased from Evonik Industries AG (Essen, Germany). Chloroform ($CHCl_3$, anhydrous, ≥99 %), dimethyl sulfoxide (DMSO, > 99 %), acetonitrile (anhydrous 99.8 %), Tween® 80, phosphate-buffered saline (PBS), rifampicin (RIF, ≥ 97 %), ciprofloxacin (CIP, ≥98 %), trifluoroacetic acid (TFA) were purchased from Sigma-Aldrich (Darmstadt, Germany). All reagents were used as received without any further purification. Tryptone soy broth (TSB) was purchased from Laboratorios Conda-Pronadisa SA (Madrid, Spain) and Tryptic Soy Agar (TSA) plates were obtained from Avantor VWR (Radnor, US). *S. aureus* ATCC 25923 was purchased from Ielab, (Alicante, Spain) and *E. coli* S17 was kindly donated by Dr. Jose A. Ainsa (University of Zaragoza, Spain). HaCaT human keratinocytes were gifted by Dr. Pilar Martín-Duque (University of Zaragoza, Spain) whereas human dermal fibroblasts (NHDF-Ad) were obtained from Lonza (Basel, Switzerland). J774A.1 mouse monocyte-macrophages ATCC-TIB-67™ were acquired from LGC Standards (Barcelona, Spain).

2.2. Materials synthesis

Fibers and particles were synthesized using a Yflow 2.2 D500 electrospinner (Málaga, Spain). For the preparation of the loaded fibers (RIF/RS100), RS100 (30 % w/v) and RIF (2.5 wt% referred to the polymer weight) were dissolved in 5 mL of $CHCl_3$ and then mixed for 30 min. In order to obtain single antibiotic-loaded fibers, the 30 % RS100 dissolved polymer containing 2.5 wt% RIF was introduced into a 10 mL syringe and fed with a flow rate of 1 mL/min in the electrospinner. The distance between the tip and the flat collector was set at 15 cm and the voltage difference at 20–23 kV. In the case of the CIP loaded particle (CIP/RS100) synthesis, RS100 (13 % w/v) was dissolved in 5 mL of $CHCl_3$ and CIP (15 wt.% referred to the polymer weight) was firstly dissolved in 200 μL of TFA and then added to the RS100 solution and mixed for 24 h at room temperature. The solution mixture was stabilized by adding Tween® 80 (0.5 % w/v). The 13 % RS100 dissolved polymer containing 15 wt.% CIP solution used for the single antibiotic particles synthesis was also introduced into a 10 mL syringe, and the flow rate was set at 0.5 mL/h, the distance between the tip and the flat collector was set at 7 cm while the voltage difference was 15–20 kV. Both RIF-loaded fibers and CIP-loaded particles were synthesized at room temperature with a relative humidity of 30–50 %.

On the other hand, a rotating drum collector (100 rpm) was used to obtain the dressings containing RIF loaded fibers decorated with CIP

loaded particles (RIF-CIP/RS100). First, the 30 % RS100 polymer solution containing 2.5 wt.% RIF in $CHCl_3$ (5 mL) was electrospun on the collector with a syringe pump working at 1.0 mL/h flow rate. The distance between the tip of the needle and the collector was fixed at 15 cm and the voltage applied was in the range +7–9 kV and the negative voltage connected to the collector varied between 2 and 4 kV. Homogeneous mats of RIF-loaded RS100 nanofibers were obtained after 3 h of electrospinning. Then, the 13 % RS100 polymer solution containing 15 wt.% CIP in $CHCl_3$ + TFA + Tween® 80 (5 mL) was electrosprayed onto the previously deposited RIF-loaded fibers using a flow rate of 1.0 mL/h. The distance from the tip of the needle to the collector was 22 cm. The voltage applied to the collector was –3–4 kV and the voltage applied to the needle was +13–14 kV. Particle-decorated fibers were obtained after 3 h of electrospraying. The process was carried out at room temperature with a relative humidity of 20–30 %.

2.3. Physico-chemical characterization

The morphology of the obtained particles, fibers and combined mats (composed of both fibers and particles), as well as the distances between fibers, were analyzed by scanning electron microscopy (SEM) to analyze the mats structure and porosity. Samples were sputtered with a Pd layer before observation and images were acquired with an Inspect F50 FEG scanning electron microscope (FEI company, Hillsboro, US). Fiber and particle diameters were measured separately (N = 150) using the ImageJ 1.53a software, and diameters of fibers and particles combined on the same mat were also measured by the use of the DigitalMicrograph® software (Version 2.31.734.0). The thickness of the dressings, both with and without RIF-CIP, was measured at three distinct points in three separate samples using a Baxlo micrometer (Germany).

To evaluate potential drug-polymer interactions, Fourier-transform infrared (FTIR) spectra were recorded using a Bruker VERTEX 70 FTIR spectrometer (Bruker, Billerica, US) equipped with a Golden Gate diamond ATR accessory. Spectra were recorded by averaging 40 scans in the 4000–600 cm^{-1} wavenumber range at a resolution of 4 cm^{-1}.

The mechanical characteristics of the RIF-CIP/RS100 mats were assessed through a tensile test conducted at room temperature utilizing an Instron Microtester 5548 along with a video extensometer laser (at a rate of 1 mm/min, with a 1 KN load cell; Instron, Norwood, US). The test samples (N = 5) were prepared in accordance with the UNE-EN ISO 527–1:2012 standard (Plastics: Determination of tensile properties) and were cut into strips measuring 50 mm × 5 mm. The tests were performed using a full-scale load of 20 N and a maximum extension of 100 mm.

Contact angle measurements were employed as a means to evaluate the hydrophobic properties of the RIF-CIP/RS100 mats. A droplet of distilled water was deposited onto the surface of the fibers, followed by precise contact angle measurements utilizing a Dataphysics OCA equipment (Dataphysics Instruments GmbH, Filderstadt, Germany) under room temperature conditions. Contact angle measurements were conducted in triplicate.

2.4. Antibiotic loading and encapsulation efficiency

Three independent samples of fibers and particles were individually dissolved in DMSO. Then RIF and CIP loadings were determined by UV–Vis spectrophotometry (Jasco V670, Jasco Applied Science, Eschborn, Germany) at the wavelengths of 340 and 280 nm, respectively.

RIF and CIP loadings in the combined mats (composed of both fibers and particles) were determined by UHPLC using a Waters Acquity equipped with a Waters 2998 Acquity PDA, C18 excel column (3 μm, 4.6 × 100 mm) at a wavelength of 280 nm (Waters, Milford, US). In this case, 2 mg of fibers decorated with particles were dissolved in an acetonitrile/water (2:1) mixture, then each sample was filtered through a 0.22 μm filter CLARIFY-NY (Phenomenex, Torrance, US). The encapsulation efficiency (EE) and the drug loading (DL) were calculated with eq. 1 and 2, respectively:

$$EE(\%) = \frac{Mass\ of\ entrapped\ drug(mg)}{Mass\ of\ drug\ added(mg)} x100 \quad (1)$$

$$DL(\%) = \frac{Mass\ of\ entrapped\ drug(mg)}{Total\ mass\ of\ combined\ mats(mg)} x100 \quad (2)$$

2.5. Drug release kinetics

In vitro release of RIF and CIP from the combined mats was performed at two different pH (5.5 and 7) to take into account the physiological pH changes during infection and wound healing. This *in vitro* release study was carried out by immersing 5 mg of the resulting material in 5 mL of a solution at pH 5.5, which was prepared using sodium acetate (2.05 g), acetic acid (1.5 mL), and NaOH 2 N. For pH 7, a solution of PBS with 2 % of Tween® 80 was used. Samples were stirred during the release study using a J.P. Selecta Movil-Rod rotating shaker (Selecta, Cham, Switzerland) at 37 °C. At determined time intervals, 1 mL of the supernatant was collected, centrifuged for 1 min at 3000 rpm and filtered with a 0.22 μm filter CLARIFY-NY. An equal volume of fresh PBS-Tween® 80 solution for pH 7 or the pH 5.5 buffer solution was replenished in the original volume. CIP and RIF released from six different samples were individually analyzed with the UHPLC system described before. The morphological effect that PBS exerted on the material was studied by immersing the combined mats during 48 h in PBS. After drying overnight the samples were observed by SEM after being sputtered with Pd. Drug release was determined up to 48 h regarding the potential clinical use of the combined mats as dressings are commonly replaced three times per week for hygienic reasons and to avoid wound fluids to soak through [20,21].

2.6. In vitro biological analyses

2.6.1. MIC and MBC

First, the antibacterial activity of free RIF and CIP individually was evaluated against *S. aureus* ATCC 25923, as a model of a Gram-positive bacteria, and against *E. coli* S17 strain as a model of a Gram-negative bacteria. Both microorganisms were grown overnight in tryptic soy broth (TSB) at 37 °C under continuous shaking (150 rpm) until reaching the stationary growth phase, afterwards they were diluted in TSB until reaching 10^5 CFU/mL. The inoculum was placed into tubes containing a specific quantity of RIF (0–0.5 ppm for *S. aureus* and 0–60 ppm for *E. coli*) dissolved in 2 % (v/v) DMSO and CIP (0–1.25 ppm for *S. aureus* and 0–0.05 ppm for *E. coli*) dissolved in sterile water. After 24 h at 37 °C and 150 rpm of incubation stirring rate, the standard serial dilution method was used to determine viable bacteria [22]. As positive control, untreated *S. aureus* and *E. coli* S17 was also included and a toxicity control using only DMSO / sterile water was also performed.

MIC and MBC (minimum bactericidal concentration) for the RIF-loaded electrospun mats coated with CIP-loaded particles (RIF-CIP/RS100) were tested and compared to equivalent doses of the free antibiotics in a physical mixture following a previously reported method [23]. Briefly, those combined mats were cut (0.02–1 mg) and placed in 24-well plates after sterilization under UV light (30 min for each side). Subsequently, 60 mL of warm TSA (47 °C) with 2 % of Tween® 80 were inoculated with 10^5 CFU/mL of the selected bacteria (*S. aureus* or *E. coli*). Then, each well of the plate containing the mats was filled with 2 mL of the inoculated TSA and incubated in a closed box with water (to keep an adequate humidity and avoid desiccation) at 37 °C for 24 h. Each sample was transferred to a Falcon type flask and 18 mL of TSB were added. Afterwards, the mixture was sonicated for 15 min and vortexed for 1 min to detach bacteria. The standard microdilution method was used to determine viable bacteria. Control samples were also included (only bacteria and bacteria treated with non-loaded mats) and each experiment was performed in triplicate with two replicas each

(N = 6).

2.6.2. Synergy studies by Fractional inhibitory concentration index (FICI) determination

The *in vitro* interactions of both antibiotics (RIF and CIP) were evaluated by the microdilution checkerboard method [22]. The assays were performed in 96-well plates, for each strain of bacteria (*S. aureus* and *E. coli*) a stock solution containing four times the MIC (4 MIC_0) of both antibiotics (RIF and CIP) was prepared. RIF was diluted two-fold in horizontal direction and CIP was diluted two-fold in vertical direction. 10 μL of bacteria (10^5 CFU/mL) (*S. aureus* or *E. coli*) were added in each well and a mirror plate without bacteria was used as negative control. The plates were incubated for 24 h at 37 °C and turbidity was observed by naked eye inspection. The assay was performed in triplicate. FICI values were calculated using the following equations (Eq. 3, 4 and 5):

$$FICI = FIC_{RIF} + FIC_{CIP} \tag{3}$$

Where.

$$FIC_{RIF} = \frac{MIC_{RIF} in\ presence\ of\ CIP}{MIC_{RIF}} \tag{4}$$

$$FIC_{CIP} = \frac{MIC_{CIP}\ in\ presence\ of\ RIF}{MIC_{CIP}} \tag{5}$$

Antibiotic synergy was identified as synergy (FICI < 0.5), addition (0.5 ≤ FICI ≤ 1), indifference (1 < FICI ≤ 4) or antagonism (FICI > 4).

2.6.3. Biofilm formation prevention and biofilm elimination

The effect of free RIF and CIP and the combined mats (RIF-CIP/RS100) against the formation of *S. aureus* and *E. coli* biofilms and the disruption caused on already formed mature biofilms were analyzed. *S. aureus* (ATCC 25923) and *E. coli* (S17) were cultured overnight until reaching stationary phase. Two different procedures, with the combination of the free drugs at equivalent doses at those loaded within the combined mats, were carried out:

- Biofilm inhibition: 10^7 CFU/mL of both bacteria was put in contact in 24-well plates with the combination of the free drugs and with different weights of the combined mats (RIF-CIP/RS100) to reach concentrations in the wells from 0.05 to 4 mg/mL and incubated for 24 h at 37 °C without shaking.
- Biofilm disruption: 10^7 CFU/mL of both bacteria were grown in well plates at 37 °C without shaking. After 24 h, planktonic cells were removed and wells containing already formed bacterial biofilms were washed twice with PBS. Then, the combination of the free drugs and different weights of the combined mats (RIF-CIP/RS100) to reach concentrations in the wells from 0.05 to 4 mg/mL along with fresh medium were added to preformed biofilms and incubated for 24 h at 37 °C without shaking.

After incubation (24 h at 37 °C), medium was discarded and resulting biofilms were washed twice with PBS and disrupted by sonication (15 min, 200 W; Ultrasons, JP Selecta, Barcelona, Spain) to count (CFU/mL) viable bacteria by the standard dilution method. Untreated bacteria and antibiotic-free mats were also tested as controls.

The crystal violet assay was also carried out to confirm the formation and disruption of the biofilm after treatment. After the biofilm formation, each well was washed twice with 1 mL of PBS. Subsequently, each well was stained with 250 μL of a 0.1 % (w/v) crystal violet solution for 10 min at room temperature. Following this, each well was washed four times with 1 mL of sterile PBS and allowed to air dry. Afterwards, 200 μL of 30 % acetic acid was added to each well, ensuring the solubilization of the stain by covering the plates. After 15 min of staining, the plate was measured using a microtiter plate reader Varioskan LUX microplate reader (Thermo Scientific, Waltham, US) at 595 nm. Each strain was tested three times, and the quantities of biofilm production were reported as the mean absorbance values of the six replicate tests. Biofilm formation was evaluated by comparing the absorbance value of the treated biofilms with that of the untreated ones (used as a control, representing 100 % biofilm stained).

2.6.4. Cytotoxicity on eukaryotic cells

To determine the cytotoxic effect of the combined mats (RIF-CIP/RS100), J774 murine macrophages, HaCaT keratinocytes and human dermal fibroblasts were used as models of mammalian somatic cell lines. All cell lines were grown in high-glucose Dulbecco's modified Eagle's medium (DMEM w/ stable glutamine, Biowest, Nuaillé, France) supplemented with 10 % (v/v) fetal bovine serum (FBS, Gibco, Waltham, US) and 1 % (w/v) antibiotic–antimycotic solution (penicillin–streptomycin-amphotericin B, Biowest, France) at 37 °C and 5 % CO_2.

The Blue Cell Viability Assay (Abnova, Taiwan) was used to measure the cell metabolism associated with cell viability. After 24 h at 37 °C, cell cultures, treated with the combined mats (RIF-CIP/RS100) to reach concentrations in the wells between 0.05 and 2 mg/mL, were incubated with the reagent (10 % (v/v) in DMEM) for 4 h at 37 °C, 5 % CO_2. After that, fluorescence was measured (530/590 nm excitation/emission) in a Varioskan LUX microplate reader (Thermo Scientific, Waltham, US). The cytotoxic effect was evaluated by comparing the fluorescence value from the treated cells and the one of untreated cells (as control, 100 % viability). Four replicas of each concentration were tested in triplicate.

2.7. In vivo studies

2.7.1. Murine excisional wound splinting model and chronic infection

In vivo experiments were carried out in compliance with the Spanish Policy for Animal Protection RD53/2013 which meets the European Union Directive 2010/63, and under Project License PI59/22 approved by the Ethics Committee for Animal Experiments of the University of Zaragoza (Spain). Mice were daily weighed and checked their general welfare prior to the surgery until the end of the *in vivo* study. Ten- to twelve-week-old diabetic obese mice ($Lepr^{db}$/$Lepr^{db}$, Janvier Labs, France) were maintained in specific pathogen-free conditions with *ad libitum* access to water and food. Diabetic mice were chosen in this study to induce chronic non-healing wounds because diabetes impairs wound healing [24]. A total of twenty-four mice were distributed in 4 experimental groups (N = 6, 3 females and 3 males):

I) Infected mice without any treatment (control group).
II) Infected mice treated with RIF-CIP/RS100 (1.4 mg).
III) Infected mice treated with a combination of free RIF and CIP (25 μL containing 2.47 μg/mL RIF and 0.33 μg/mL CIP in PBS).
IV) Infected group treated with the model antiseptic in clinical practice, chlorhexidine (CHXD; 25 μL at a concentration of 10 mg/mL as we previously reported [25]).

The mouse excisional wound splinting model was carried out following a previously established protocol [25]. In brief, mice were anesthetized using a facemask with 5 % isoflurane, and maintained with 1.5–2 % isoflurane with a 1 L/min oxygen flow. Then, the inter-scapular area was shaved and disinfected with 70 % ethanol (v/v). Next, Meloxicam (5 mg/kg w/v) was subcutaneously administered and maintained until 72 h post-surgery and infection (PSI). A full-thickness wound was made in the inter-scapular area using a sterile 8-mm punch biopsy tool (Eickemeyer Veterinary Equipment Ltd., Stratford, Canada). A ring-shaped silicone wound splint (14 mm OD × 10 mm ID × 0.5 mm thick; Grace Bio-Labs, Bend, US) was sutured around the wound (Dafilon 4/0; Braun, Germany) to prevent its closure. Subsequently, the wound was infected with a dispersion of *S. aureus* ATCC 25923 (25 μL, ≈10^7 CFU/mL in PBS). Lastly, the wound was covered with a sterile adhesive plaster (Hartmann, Heindenheim, Germany) and Tegaderm™

(3 M, Saint Paul, US) to protect and facilitate the development of a chronic infected wound. These conditions were maintained until 21 days PSI, with the animals' welfare being daily evaluated.

2.7.2. Wound treatment, infection evaluation and histopathological analysis

After the initial 21 days PSI period, the wounds were treated every 24 h as described by the respective experimental groups until 28 days PSI. Additionally, wound infections were monitored by collecting microbiological samples using a swab (Deltalab, Barcelona, Spain) from the wounds at 21, 24 and 28 PSI, which were then cultured on agar plates. At 28 days PSI, euthanasia was performed by CO_2 inhalation. Lastly, wounds were collected along with the surrounding tissue, fixed in PBS with paraformaldehyde (4 % w/v) (Alfa Aesar, Heysham, UK) for 24 h, and embedded in paraffin. Histological sections (5 μm) were stained with hematoxylin and eosin (HE) for pathological analysis.

2.8. Statistical analyses

The results are presented as the mean ± standard deviation (SD). In vitro biological experiments were analyzed using two-way analysis of variance (ANOVA) with GraphPad Prism 9 (San Diego, US). Statistically significant differences were considered when $p \leq 0.05$. The nanoparticle characterization experiments were performed three times, while the bactericidal analysis experiments and biofilm analysis were each conducted in triplicate and quadruplicate, respectively.

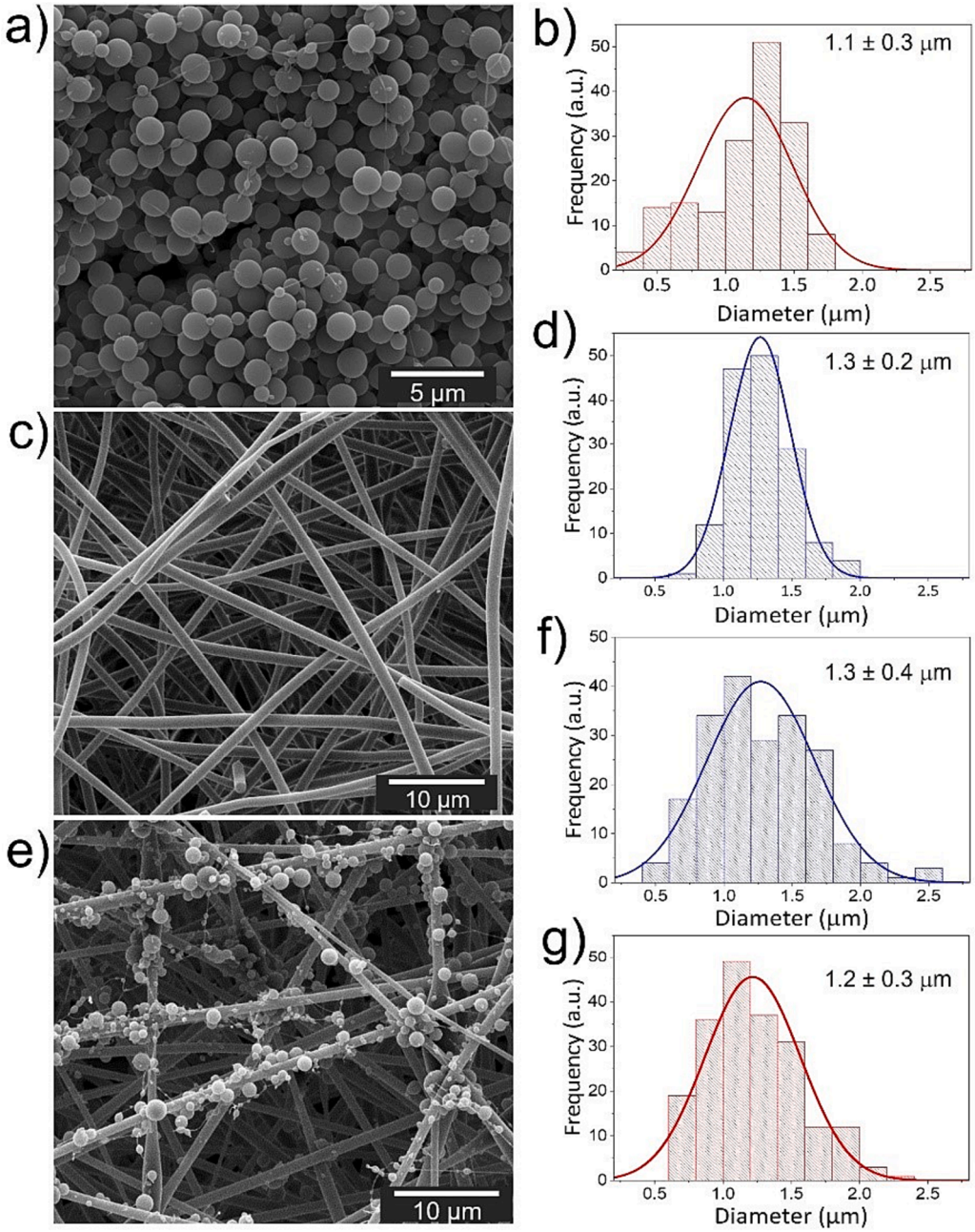

Fig. 1. Morphological characterization of the synthesized materials: a) SEM image and b) size distribution of CIP/RS100 particles; c) SEM image and d) size distribution of RIF/RS100 fibers; e) SEM image, f) fibers size distribution and g) particles size distribution in the RIF-CIP/RS100. Size was retrieved from SEM measurements (N = 200).

3. Results and discussion

3.1. Materials physicochemical characterization

According to the SEM results, CIP loaded microparticles deposited in the collector had spherical morphology with an average diameter of 1.1 ± 0.3 μm (Fig. 1 a, b). Antibiotic-free Eudragit® RS100 microparticles prepared using the same precursor solution ($CHCl_3$ + TFA + Tween 80) had a particle size distribution centered at 1.4 ± 0.5 μm (results not shown), therefore, the presence of the CIP in the electrospinning solution would not produce any major change in the resulting particle size. RIF loaded fibers showed a mean diameter centered at 1.3 ± 0.2 μm (Fig. 1 c, d), very similar to the one of empty fibers (1.1 ± 0.3 μm, results not shown). RIF encapsulation efficiency according to UV-Vis results was very high showing values around 97 % (Table 1). Different RIF concentrations in the polymeric precursor solution from 2.5 to 10 % w/w (referred to the polymer weight) were studied, but only the lowest concentration allowed a stable Tayloŕs cone during electrospinning, and as a consequence, the drug loading achieved in the fibers was only 2.3 ± 0.07 % w/w.

The main limitation in the encapsulation of CIP in the particles was the insolubility of this antibiotic in the organic polymeric solution due to its high hydrophilicity at acidic pH. When dissolving in acidic aqueous solution, a coaxial electrospray was needed and the flow rate of this aqueous solution was very low (0.05 mL/min) to avoid the Taylor's cone destabilization. To solve this problem and increase the antibiotic encapsulation, CIP was first dissolved in TFA. Then, an emulsion of this solution in the chloroform-based polymeric solution stabilized with Tween 80 was prepared. This method allowed to obtain a high drug loading in the precursor solution (15 % w/w referred to the polymer weight) and since the encapsulation efficiency was 86.9 ± 6.9 %, the final drug loading was as high as 11.0 ± 1.0 w/w.% (Table 1). The obtained CIP loading was higher than the one reported by Dillen et al. [26] for Eudragit® RS100 particles synthesized by the w/o/w emulsification solvent evaporation technique followed by high-pressure homogenization. These authors achieved around 65 % w/w EE using only Eudragit® RS100 but they obtained an increase up to 70 % w/w only when combining this polymer with PLGA. On the other hand, CIP loaded chitosan particles generated by electrospraying had higher drug loadings than the ones here reported, around 15 % w/w, but with lower EE (76 %) [27]. To the best of our knowledge, there are no previous reports on the synthesis of CIP/RS100 loaded particles obtained by electrospraying.

As we mentioned before, electrospun fiber-based dressings have many advantages that make them ideal as wound healing promoters. Their high surface area and tortuosity provide a physical barrier against bacterial penetration, but still retaining the oxygen and water vapor transfer ability necessary for wound healing keeping an adequate moisture while avoiding maceration [28]. One intended approach when loading RIF and CIP into a combination dressing was to obtain a functional dressing containing both antibiotics in one step. However, the impossibility of using the same solvent to simultaneously solubilize both drugs and the polymer led to the need to load each drug independently, one within the fibers and the other one within the particles. The decoration of fibers with particles assures the access of both drugs to the releasing medium from one single medicated mat. Fig. 1e shows a SEM image of the resulting RIF loaded fibers decorated with CIP loaded particles (RIF-CIP/RS100). Even when the synthesis conditions had to be changed because of the rotating drum collector used, RIF loaded fibers average diameters (1.3 ± 0.4 μm) (Fig. 1f) were very similar to those obtained for the un-decorated ones (Fig. 1d). Deposition of particles onto the non-conductive fiber mat required the use of the rotating collector in order to obtain a homogeneous distribution. Particles mean diameters (1.2 ± 0.3 μm) (Fig. 1g) in the combined RIF-CIP/RS100 mats were also very similar to the ones obtained for the CIP-loaded microparticles deposited on the flat collector (Fig. 1b).

RIF encapsulation efficiency obtained from the fibers deposited on the drum collector was lower than that obtained from the ones retrieved on the flat collector (Table 1). This decrease from 97.1 % to 87.1 % could be related to the lower voltage needed in this case to obtain a stable Tayloŕs cone. It was reported that an increase in the voltage would produce an increase in the flow rate between the needle and the collector [29]. The lower voltage applied for fibers collected on the rotating drum would decrease the solution flow rate and, consequently, the time for the drug to diffuse and evaporate from the solution jet would be higher, increasing its loss. There is also an important decrease in the EE of CIP for the particles deposited on the fibers, again the jet travelling time was higher owing to the higher tip to collector distance in this case. In general, the longer the time from the tip of the needle to the collector, the higher the diffusion and the potential evaporation of the drug present in the solvent. The DLs in the final RIF-CIP/RS100 were 0.6 ± 0.1 wt.% (RIF) and 2.0 ± 0.1 wt.% (CIP) referred to the total weight of the combination mats.

FTIR analysis was carried out in order to confirm the presence of RIF in the loaded fibers and a possible interaction between the drug and the polymer (Fig. 2a). However, only peaks related to the Eudragit® RS100 were detected in the loaded fibers, probably attributed to the low concentration of the antibiotic present in the fibers being below the limit of detection of the technique. The presence of CIP and potential drug-polymer interactions in the loaded particles were also investigated by FTIR analysis, and in this case, its higher drug loading (see Table 1) facilitated its identification. Fig. 2b displays the FTIR spectra of Eudragit® RS100 particles (named RS100), free CIP and CIP-loaded Eudragit® microparticles (named CIP/RS100). Characteristic peaks for free CIP can be observed at 1614 and 1283 cm^{-1} due to the vibration of the phenyl framework conjugated to –COOH and the stretching vibration of the C–F bond, respectively [30]. For the CIP/RS100 particles, vibrations related to the polymer can be observed at 1722 cm^{-1} (C = O stretching), 1448 cm^{-1} (CH_2 asymmetric bending), 1384 cm^{-1} (CH_3 asymmetric bending), 1144 cm^{-1} (C-CO-C stretching) and at 1098 cm^{-1} (C-N stretching) [31]. A small peak at 1629 cm^{-1} would confirm the presence of CIP in the particles. The significant shift observed for this band would suggest drug-polymer interactions, since it is known that acidic compounds like CIP interact with Eudragit® polymers by means of electrostatic interaction between the carboxyl moiety of the drug and the quaternary ammonium groups of the polymer [26]. Similar results were observed in the RIF-CIP/RS100 FTIR spectrum (Fig. 2c) showing peaks at 1622 and 1596 cm^{-1}, that would be related to vibration of the phenyl framework conjugated to –COOH of CIP. The interaction of the antibiotic and the polymer would also be confirmed in this case by the shift observed.

The dressing composed solely of fibers and particles, without containing RIF-CIP, exhibited a contact angle of 153 ± 3.2°. On the other

Table 1
Synthesis parameters and characterization results for the obtained materials. Data are presented as mean ± SD.

		Applied voltage (kV)	Tip to collector distance (cm)	Diameter (μm)	EE (%)	DL (% w/w)
Fibers RIF/RS100		20–23	15	1.3 ± 0.2	97.1 ± 2.8	2.3 ± 0.07
Particles CIP/RS100		15–20	7	1.1 ± 0.3	86.9 ± 6.9	11.0 ± 1.0
RIF-CIP/RS100	Fibers RIF/RS100	9–13	15	1.3 ± 0.4	87.1 ± 7.6	0.6 ± 0.1
	Particles CIP/RS100	16–18	22	1.2 ± 0.3	56.1 ± 10.6	2.0 ± 0.1

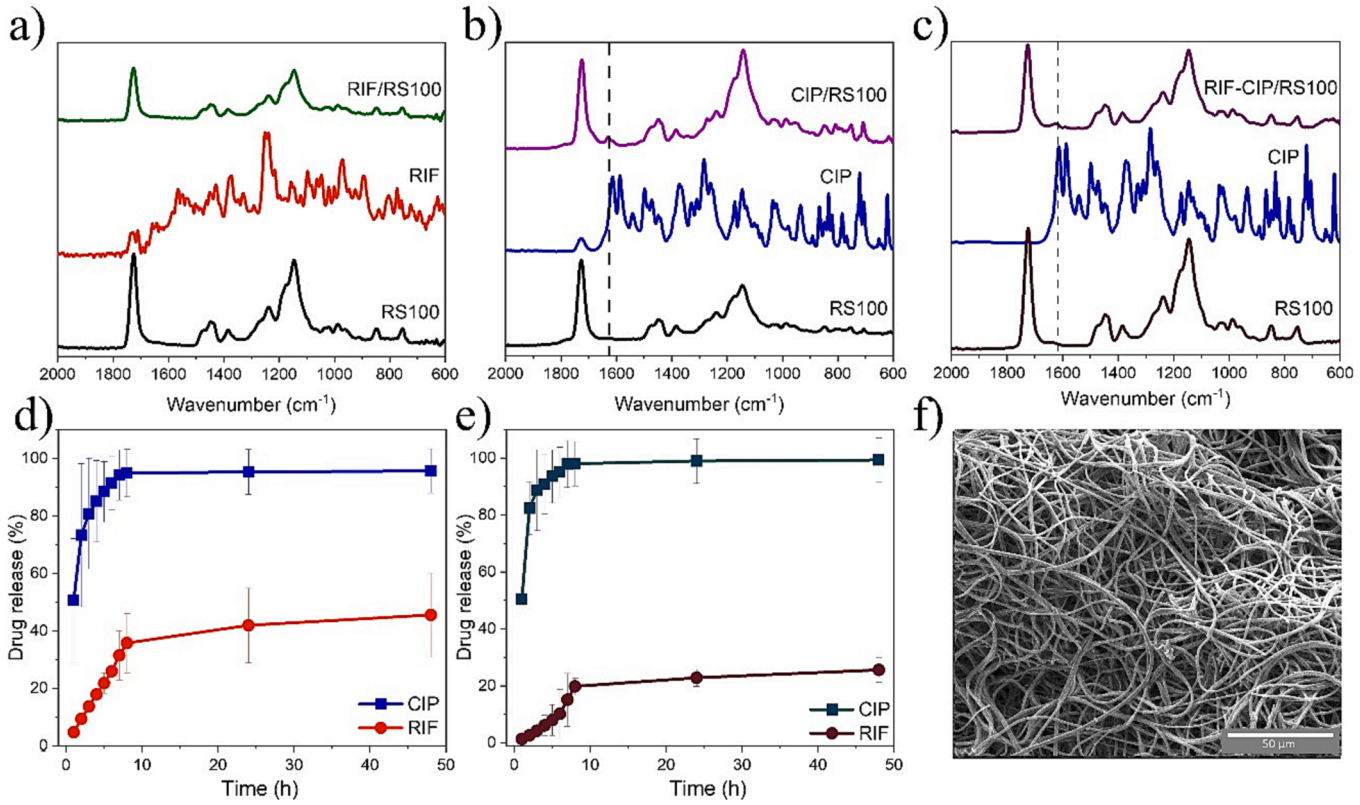

Fig. 2. Physico-chemical characterization of the synthesized materials. Comparison of FTIR spectra of: a) RS100, free RIF and RIF/RS100; b) RS100, free CIP and CIP/RS100 and c) RS100, free CIP and free RIF-CIP/RS100; d) Cumulative drug release from RIF-CIP/RS100 at pH 7; e) Cumulative drug release from RIF-CIP/RS100 at pH 5.5; f) SEM micrograph of the morphology of the wound dressing after drug release for 50 h at pH 5.5.

hand, the dressing incorporating RIF-CIP displayed a contact angle of 146 ± 2.1°. This demonstrates that the mat maintained its hydrophobic nature in the absence and presence of RIF-CIP. This hydrophobic surface would prevent from the wound fluid to soak through and would favor blood clotting. In addition, due to the large porosity of the antibiotic-loaded electrospun dressings here fabricated (33 ± 9 μm average pore size between fibers), their reduced thickness (38 ± 4 μm) and reduced tortuosity, a large oxygen and water vapor permeability is envisaged; therefore water vapor exchange would be promoted through the porous mats avoiding wound maceration.

The pore size, measured by quantifying the distances between fibers by SEM, was determined to be 31 ± 10 μm for the drug-free dressing, very similar to the one of the RIF-CIP/RS100 mats (33 ± 9 μm). The thickness of the drug-free dressing (35 ± 3 μm) was also similar to the one of the RIF-CIP/RS100 mats (38 ± 4 μm). Therefore, the incorporation of the antibiotics in the dressings did not change substantially the morphology of the resulting mats.

The drug-free dressing showed a Young's module of only 0.007 ± 0.0002 MPa, indicating its flexibility and elasticity. Its tensile strength of 0.45 ± 0.1 MPa demonstrated a good level of resistance to tearing or mechanical damage, and it could undergo a significant strain of 19 ± 0.45 % before breaking. Similarly, the RIF-CIP/RS100 dressings exhibited a Young's module of 0.004 ± 0.0001 MPa, confirming its flexibility which could be advantageous to easily adapt and conform with the wound contour. Its measured tensile strength was 0.28 ± 0.1 MPa, and it could endure a strain of 16 ± 0.5 %. These results suggest that RIF-CIP/RS100 dressings possess characteristics favorable for wound application, as they are mechanically adaptable, facilitating an easy and comfortable dressing application to the wound contour.

Fig. 2d and 2e display the RIF and CIP release profile from RIF-CIP/RS100 mats at pH 7 and 5.5, respectively. About 95 % of the loaded CIP was released in the first 8 h at both pHs tested and then drug release was stabilized reaching a plateau. The initial release would be related to the dissolution and the fast diffusion of the hydrophilic antibiotic from the superficial particles in contact with the aqueous release medium despite the pH of the medium. CIP present in the outmost part of the microparticles was rapidly released and a slower sustained release of the RIF in the solid matrix structure of the fibers after matrix erosion was observed. Then, we postulate that RIF slow release from the core of the fibers would provide an extended duration of the antimicrobial prophylactic action. This release kinetics is very appropriate to eradicate first intruding bacteria preventing colonization thanks to the immediate availability of CIP, and then the sustained RIF release could inhibit the growth of any remaining bacteria and prevent from a potential re-infection. RIF release at both pH was lower than that obtained from CIP, observing at pH 7 in the first 8 h that the release only reached 35 % of the total loaded drug and then it slowly increased up to 45 % after 50 h. On the other hand, at pH 5.5 RIF release was almost half (20 % of the loaded antibiotic) and also slowly increased up to 25 % after 50 h (Fig. 2e). These results are in agreement with previous studies concerning the lower solubility of RIF at pH 5.5 compared to that at physiological pH [32]. RIF release kinetics may be probably attributed to its reduced aqueous solubility (i.e., just sparingly soluble in aqueous buffers) and due to the slower erosion of the fibers compared to the microparticles due to the lower surface per volume ratio of the former. In this line, SEM micrographs of the mats showed that the structure and morphology of the mats were preserved after immersion in the release medium and performing the drug release analysis for 50 h indicating their mechanical stability as wound dressing and that they could be easily removed after use (Fig. 2f). In addition, RIF-CIP/RS100 mats would retain a large amount of RIF to produce an extended prophylactic effect. The different aqueous solubility of both antibiotics, the different drug loading in the particles and the fibers and their different morphology (and consequent surface area exposed to the release

medium) would explain the drug release kinetics observed.

3.2. In vitro biological studies

3.2.1. Free antibiotics activity in planktonic cultures

The bactericidal activity of both antibiotics was tested against *S. aureus* and *E. coli* planktonic cultures as Gram-positive and Gram-negative models, respectively. MIC and MBC values (Table 2) found in *S. aureus* cultures for CIP (MIC 0.25 μg/mL, MBC 1 μg/mL) were similar to those reported in the previous literature (MIC 0.5 μg/mL, MBC 1 μg/mL) [33] as well as those obtained for RIF (MIC < 0.05 μg/mL, MBC 0.5 μg/mL) against *S. aureus* ATCC 25923 [34]. It is well-known that CIP possesses strong activity against Gram-negative bacteria [35], as a consequence MIC and MBC values against *E. coli* were very low (MIC 0.005 μg/mL, MBC 0.01 μg/mL). The characteristic outer cell-protecting membrane of Gram-negative represents an effective barrier for polar molecules and being CIP a highly water-soluble antibiotic its effect against *E. coli* is promoted. On the other hand, RIF is mainly used to treat infections against Gram-positive pathogens [36] showing higher concentrations needed to inhibit growth or eliminating Gram-negative bacteria (MIC 20 μg/mL, MBC 40 μg/mL) [37]. Again, due to the non-polar nature of RIF, probably the penetration of RIF through the outer membrane of Gram-negative bacteria would be largely excluded compared to Gram-positive bacteria.

3.2.2. Synergism

As mentioned before, antibiotic combinations attempt to prevent or delay the *in vivo* emergence of drug-resistant subpopulations of pathogenic microorganisms. Additionally, RIF should not be used as mono therapy because of the rapid development of resistance, therefore, its combination with CIP could provide a successful treatment at lower doses than the ones required for the monotherapy alone [38]. To evaluate the potential presence of synergism between both antibiotics, the FICI was calculated (Fig. 3a and b). The FICI values of both antibiotics against *S. aureus* and *E. coli* (0.10 and 0.14, respectively) indicated that the combination of RIF and CIP exerted a synergistic effect (≤0.5) [39]. As indicated in Table 2, against the Gram-positive bacteria, the MIC of RIF could be reduced from 0.05 to 0.001 μg/mL (i.e., 50 times reduction) in combination with CIP, while only 0.02 μg/mL of CIP in the combination exhibited the same effect as 0.25 μg/mL of CIP alone (i.e., 12.5 times reduction). Against *E. coli*, the concentration of RIF could be decreased from 20 to only 2 μg/mL (i.e., 10 times reduction) when in combination with 0.002 μg/mL of CIP (i.e., 2.5 times reduction) to obtain the MIC values of the combination of both antibiotics. According to these results, the concentration of both antibiotics needed to inhibit Gram-positive and Gram-negative bacterial growth would be lower when loaded simultaneously in the system than when used independently. Therefore, the combination therapy here proposed would successfully reduce the doses needed to eliminate a wide spectrum of pathogenic bacteria present and thus, lowering the possibility of the development of bacteria resistances and the chronicity of infections.

3.2.3. System antibacterial activity

Wound dressings containing several drugs were previously reported in the literature. For instance, a system consisting of fibers loaded with the antibiotic mupirocin and fibers loaded with the anesthetic lidocaine were prepared through a dual spinneret [40]. The anesthetic lidocaine was also loaded with tetracycline by coaxial electrohydrodynamic printing [41]. The synthesis of electrospun nanofibers loaded with two antibiotics, GS and CIP, was also reported [16]. In that study, the dual drug loaded fibers showed a complete release of GS in 6 days and a sustained release of CIP for over three weeks with a significant reduction in the bacterial counts in the wound bed using a murine model of a deep burn infected with *P. aeruginosa*. The rapid release of GS and extended release of CIP accelerated the wound healing process while controlling the infection. Other authors have recently showed the synthesis of electrospun chitosan/poly(vinyl alcohol) nanofibers loading colistin and meropenem, which displayed synergistic bactericidal effects against XDR clinical isolates of *Acinetobacter baumannii,* as well as *in vitro* and *in vivo* significant biocompatibility [17].

Table 2
MIC and MBC of free ciprofloxacin (CIP) and rifampicin (RIF), as well as when added in combination (CIP-RIF) (N = 12).

	S. aureus ATCC 25923		*E. coli* S17	
	MIC (μg/mL)	MBC (μg/mL)	MIC (μg/mL)	MBC (μg/mL)
CIP	0.25	1.0	0.005	0.01
RIF	< 0.05	0.5	20	40
RIF-CIP	RIF 0.001	–	RIF 2.0	–
	CIP 0.02	–	CIP 0.002	–

The inhibitory and bactericidal effects of RIF-CIP/RS100 were evaluated against *S. aureus* and *E. coli* strains in solid TSA cultures. Fig. 3c and d show the antimicrobial activity depending on the concentration of the mat (total weight of the mat (0.02–1 mg) in the volume of medium where the bacterial inoculum is present (2 mL)) and compared to equivalent doses of the same antibiotics in a physical mixture. The concentration of both antibiotics in the mixture was equivalent to the concentration released from the RIF-CIP/RS100 combinatorial system in 24 h. In this case, 0.05 mg/mL of RIF-CIP/RS100 were necessary to inhibit *S. aureus* and *E. coli* growth (Fig. 3c and 3d). According to the antibiotic release studies (Fig. 2), this combinatorial system was able to release after 24 h 0.90 and 0.12 μg/mL of CIP and RIF, respectively. To completely eradicate both bacterial strains, it was necessary to use 0.1 mg/mL of RIF-CIP/RS100, releasing, according to the drug kinetic release analysis, 1.9 and 0.25 μg/mL of CIP and RIF, respectively after 24 h. Even though the concentration of CIP released from the system was higher than that required for the individual antibiotics to eradicate *S. aureus* and *E. coli* (Table 2; ≤ 1 μg/mL), the concentration of RIF needed to achieve a complete eradication of bacteria (0.25 μg/mL) was highly decreased against the Gram-negative bacteria (Table 2; 40 μg/mL) while it was reduced by half (Table 2; 0.5 μg/mL) against the Gram-positive one. This dose reduction needed to fully eliminate the pathogenic bacteria when combining both RIF and CIP in the same dressing would outperform the application of both antimicrobials alone while preventing the chronicity of infection and the evolutionary selection of resistant strains. It should be noted that the RS100 system (not loaded with antibiotics) exerted no bactericidal effects yielding the same bacteria counts as the control samples depicted in Fig. 3c and 3d.

3.2.4. RIF-CIP/RS100 antibiofilm activity

As we mentioned before, in many cases, following initial contaminations, microbial wound populations can colonize the wound bed and many species can associate forming biofilms that reduce the susceptibility to host defenses and to antimicrobial agents, undermining standard clinical therapies, including antibiotic therapy [42]. It has been shown that killing bacteria in a biofilm may require up to 1000 times the antibiotic dose necessary to achieve the same result in its planktonic form [43]. As previously reported, multiple species of bacteria populate chronic wounds and derived biofilms often contain one or more species of Gram-positive and Gram-negative bacteria and/or fungi [44]. The antibiofilm formation ability of the prepared system composed of RIF-loaded fibers decorated with CIP-loaded particles (RIF-CIP/RS100) was tested against *S. aureus* biofilms (Fig. 4a) showing its ability to avoid biofilm formation. The action of the drug eluting system developed was compared to the effect of the mixture of the free antibiotics at the same concentrations than those released from RIF-CIP/RS100 in 24 h. Regarding the inhibition of biofilm formation, the mixture of the free antibiotics was not able to avoid *S. aureus* biofilm formation in contrast to RIF-CIP/RS100 that, at a mat concentration of 1 mg/mL in the culture medium, successfully prevented *S. aureus* biofilm formation (Fig. 4a).

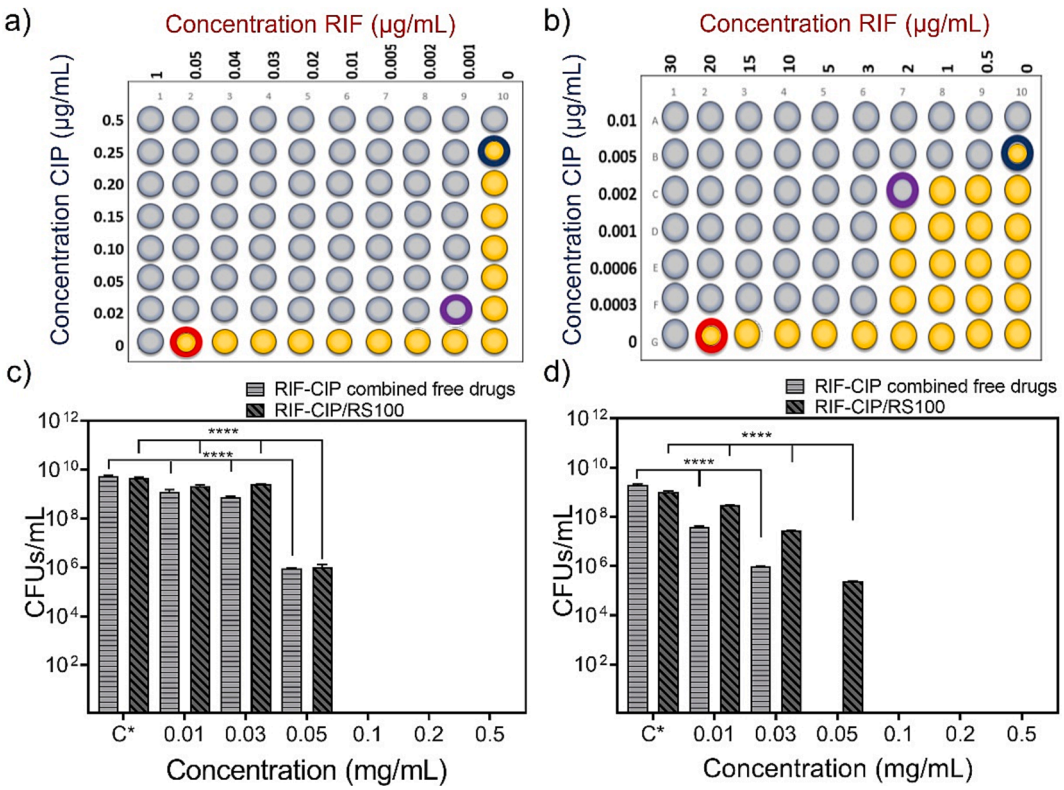

Fig. 3. Effects of the combination of both antibiotics in bacterial growth. a) and b) Fractional Inhibitory Concentration Test for *S. aureus* (a) and *E. coli* (b). The yellow wells depict areas of bacterial growth, in contrast with the grey ones that involve the absence of bacterial growth. The blue circle denotes the MIC of free CIP, while the red circle represents the MIC of free RIF and the purple circle emphasizes the observed synergistic effect (MIC values when both antibiotics were added in combination); c) and d) Bactericidal activity of a mixture of equivalent doses of the free drugs and the RIF-CIP/RS100 system against *S. aureus* (c) and *E. coli* (d). The concentration in the X axis refers to that of the RIF-CIP/RS100 combinatorial system. Data are depicted as mean ± SD of 3 independent experiments in triplicate (n = 6). Significant differences are shown between controls (only bacteria and RS100 system without antibiotics) and experimental groups (*p < 0.05; **p < 0.01; ****p < 0.0001).

This concentration was much higher than that needed to eliminate planktonic bacteria (MBC 0.1 mg/mL; Fig. 3c), results that were expected since, as we mentioned before, *S. aureus* strains embedded in biofilms are up to 1000 times less susceptible to antibiotics than their planktonic counterparts [45]. On the other hand, 2 mg/mL of RIF-CIP/RS100 were enough to completely eradicate *S. aureus* preformed mature biofilm while free antibiotics were not able to totally eliminate those biofilms (Fig. 4b), which represents an outstanding result. The better performance of the system could be related to the interaction between the cationic polymer and the bacterial biofilm. Many of the biofilm components as well as the bacterial cell envelop yield overall negative charge, which could have a strong electrostatic interaction with the quaternary ammonium groups of the Eudragit®-based polymeric surface [45]. In previous studies, it was demonstrated that the direct contact between the pathogens and the polymeric fibers was needed to exert a strong antibacterial action [46]. Conversely, the behavior of free drugs and RIF-CIP/RS100 to inhibit *E. coli* biofilm formation and to eradicate preformed biofilms is depicted in Fig. 4c and 4d, respectively. Again, the RIF-CIP/RS100 system exerted significantly higher antibiofilm activity compared to the addition of the free antibiotics as all the concentrations of the combinatorial system tested were able to avoid (Fig. 4c) or eradicate (Fig. 4d) *E. coli* biofilms. These results would indicate that *E. coli* cell damage can negatively affect cell attachment that represents the first step in biofilm formation [47]. Moreover, it could be associated to the polymer interaction with one of the extracellular polymer biofilm components, poly ß-1,6-N-acetyl-D-glucosamine, that would hinder cellular attachment and reticulation of the exopolysaccharide matrix delaying the antibiotics action [48]. Optically, in the RIF-CIP/RS100 samples we did not observe any biofilm on the air–liquid interface as expected during *E. coli* pellicle formation. Furthermore, crystal violet staining confirmed these results showing that quantitatively RIF-CIP/RS100 at 0.05 mg/mL was able to reduce biofilm formation and to eradicate mature biofilms (Fig. 4e, 4f and 4 g). Crystal violet stains both extracellular biofilm matrix and bacterial cells (i.e., total biomass) and it was clearly observed that the inhibition/eradication was enhanced for the Gram-negative bacteria. It should be noted that the RS100 system (not loaded with antibiotics) exerted no bactericidal effects yielding the same bacteria concentration as the control samples depicted. These results are very promising in the treatment of chronic wounds as biofilms derived from these wounds are usually polymicrobial and the synthesized RIF-CIP/RS100 combinatorial system was able to efficiently eliminate *in vitro* both biofilm models.

3.2.5. Cell cytotoxicity

A wound dressing should not have any negative impact on the regenerative cells that are involved during the wound healing process. In accordance with the ISO 10993–5:2009 standard [49], a compound is considered cytocompatible when cell viability remains above 70 %. To evaluate the cytocompatibility of RIF-CIP/RS100, HaCaT keratinocytes, human dermal fibroblasts and J774 macrophages were selected for the analysis. Fig. 5 shows the percentages of viable cells after being exposed to the combined free drugs (Fig. 5a), the antibiotic-free RS100 (Fig. 5b) and RIF-CIP/RS100 (Fig. 5c) after 24 h of contact compared to the control samples (not treated cells, assigned with 100 % viability). The concentrations of the combined free antibiotics used in the cytotoxicity assay (Fig. 5a) are equivalent to the concentrations released by the dressing after 24 h. In all cases, the cell viability of the three cell lines was equal or higher than 70 % at the concentrations tested which were

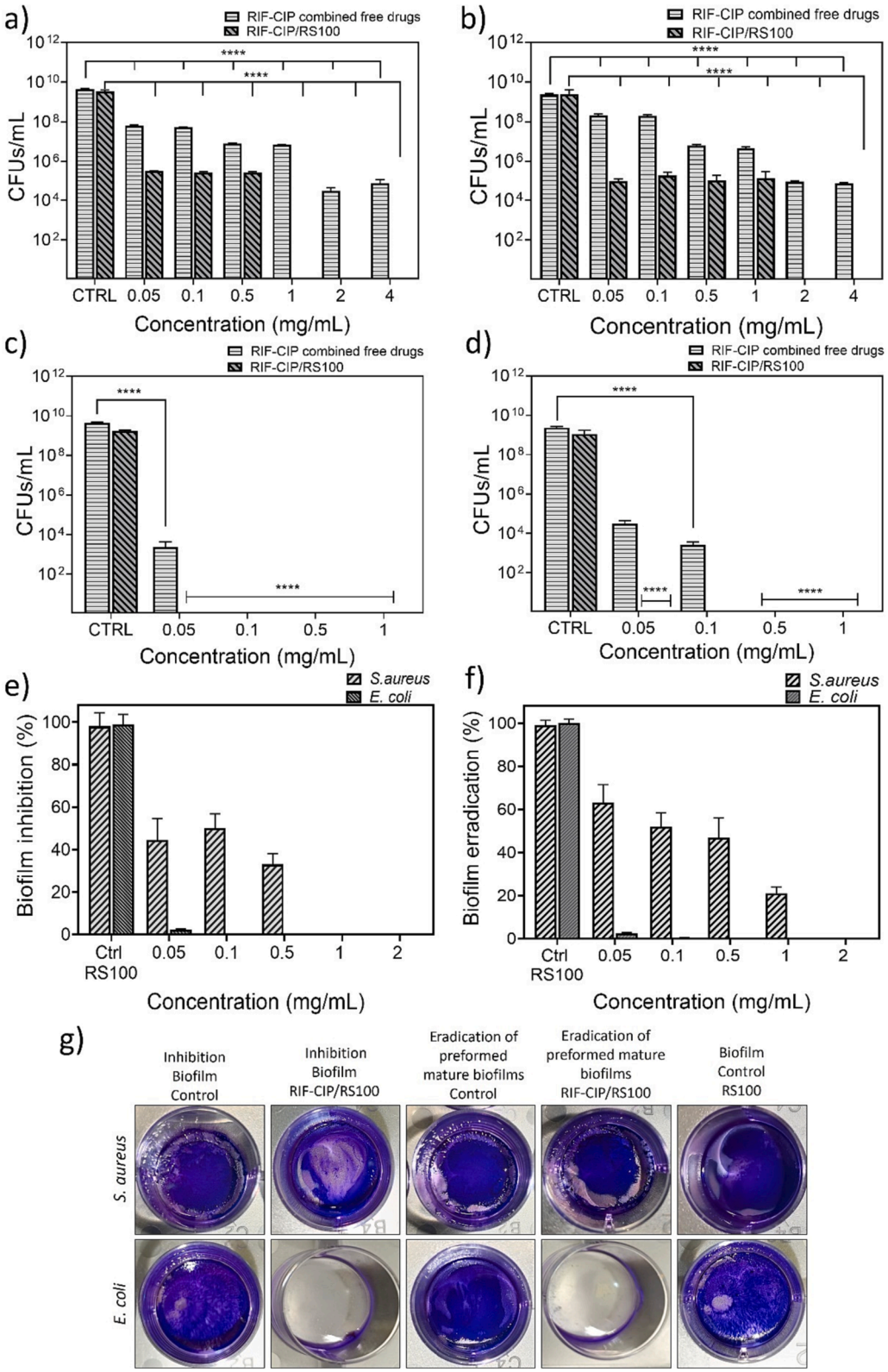

Fig. 4. Antibiofilm activity of free RIF and free CIP combined together, and RIF-CIP/RS100. a) Inhibition of *S. aureus* biofilm formation; b) Eradication of *S. aureus* preformed mature biofilms; c) Inhibition of *E. coli* biofilm formation; d) Eradication of *E. coli* preformed mature biofilms. e) Results of crystal violet staining after biofilm inhibition; f) Results of crystal violet staining after preformed biofilm eradication; g) Images showing crystal violet staining using a dressing concentration of 0.05 mg/mL. Data are depicted as mean ± SD of 4 independent experiments in triplicate (n = 12). Significant differences are shown between control and experimental groups (*$p < 0.05$; **$p < 0.01$; ****$p < 0.0001$). The drug-eluting system action was compared to the effect of the free antibiotics mixture at the same concentrations released from RIF-CIP/RS100 within 24 h. The concentration in X axis refers to that of the RIF-CIP/RS100 combinatorial system.

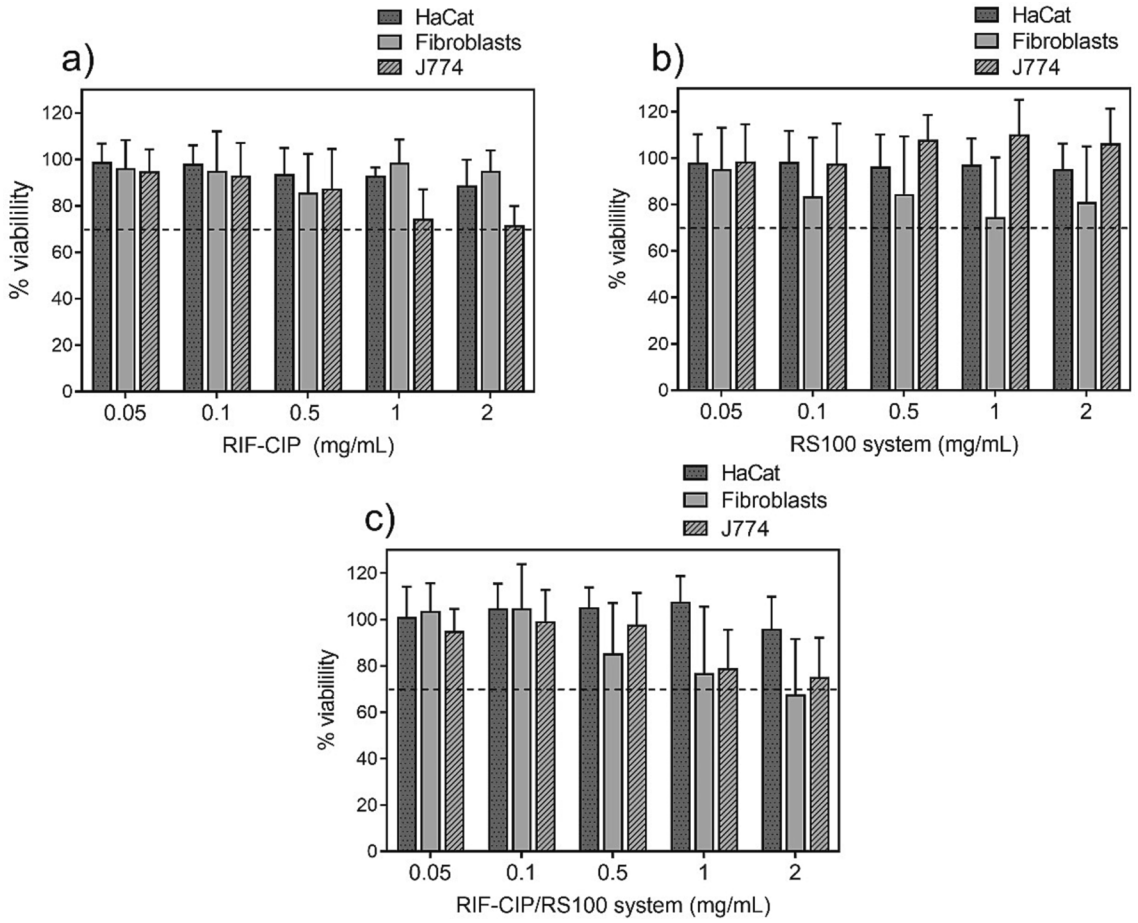

Fig. 5. Cell viability in keratinocytes (HaCaT), fibroblasts and macrophages (J774) cultures after treatment for 24 h with: a) RIF-CIP combined free drugs; b) RS100; c) RIF-CIP/RS100. The dotted line shows the threshold of 70 % of cell viability in accordance with ISO 10993–5 [49]. Control samples were considered as 100 % viability. Four replicas of each concentration were tested in triplicate (N = 12). The concentration in X axis refers to that of the RIF-CIP/RS100 combinatorial system.

in the range of those reported above as MBCs, for both planktonic and biofilms assays. Our results are in accordance with previous studies regarding the cytocompatibility of RS100 particles in human dermal fibroblasts and in Caco-2 cells even loaded with RIF at concentrations up to 20 mg/mL [34,50]; in MDCKII and human primary olfactory mucosa cells at concentrations up to 2 mg/mL [51]; and in human glioblastoma cells (U87MG) for 72 h though at lower concentrations than ours (≤24 μg/mL) [52]. Antibiotics have been also extensively shown as non-cytotoxic in different cell lines at the concentration range used in our assays [53–55]. In conclusion, RIF-CIP/RS100 was considered to be non-cytotoxic for the cell lines studied at the doses at which bacteria were eradicated. These results are very valuable for the intended application in the healing of chronic infected wounds as the integrity of patients' cells is essential to assure an adequate tissue regeneration.

3.3. *In vivo evaluation of RIF-CIP/RS100 in a chronic infected murine wound model*

The effectiveness of RIF-CIP/RS100 was evaluated in a chronic infected wound model in diabetic obese mice ($Lepr^{db}/Lepr^{db}$) developed through the murine excisional wound splinting model in which the natural murine wound closure through skin contraction is hampered to mimic the human granulation and reepithelization processes. Twenty-one days PSI, wounds were treated daily with RIF-CIP/RS100 (1.4 mg) or with the combination of free antibiotics at the same concentrations released by the mats in 24 h (2.47 μg/mL RIF and 0.33 μg/mL CIP) to clarify whether the loading of antibiotics into RS100 may improve their bactericidal activity and healing efficacy. Control groups (infected but not treated and treated with the common antiseptic CHXD) were also studied.

Fig. 6a depicts the results concerning the morphological and microbiological evaluation. At 21 days PSI, as the insets regarding bacteria load indicate, wounds were massively infected representing a chronic infected wound model. After three days of treatment (24 days PSI), RIF-CIP/RS100 and RIF-CIP significantly reduced the bacterial load up to mild bacterial growth and the wounds appeared almost closed, whereas the CHXD-treated group showed a superior bacterial load (moderate growth). Finally, the treatments successfully eradicated *S. aureus* infection at the end of the assays (28 days PSI) showing fully closed wounds and no bacteria growth though the control group still displayed moderate bacterial load. The histopathological analysis was also performed at 28 days PSI (Fig. 6b) and demonstrated that the skin was almost completely recovered after generating the chronic infected wound in all groups, with non–significant differences between them. However, when mice were treated with RIF-CIP/RS100 and RIF-CIP, they showed a low degree of dermal inflammation and, moreover, the epidermis seemed to be more recovered in the RIF-CIP/RS100 group. Mice treated with CHXD presented a higher degree of inflammatory and fibrotic reaction in the superficial dermis. Our findings confirm the *in vitro* results described above in which *S. aureus* biofilm was successfully eradicated by RIF-CIP/RS100 (Fig. 4a and 4b) also showing their cytocompatibility (Fig. 5c). These results highlight the more efficient behavior of RIF-CIP/RS100 in wound healing compared to the administration of the free antibiotics or even the common antiseptic chlorhexidine. Moreover, the *in vivo* studies confirmed the potential of our advanced medicated dressings for the treatment of these complicated

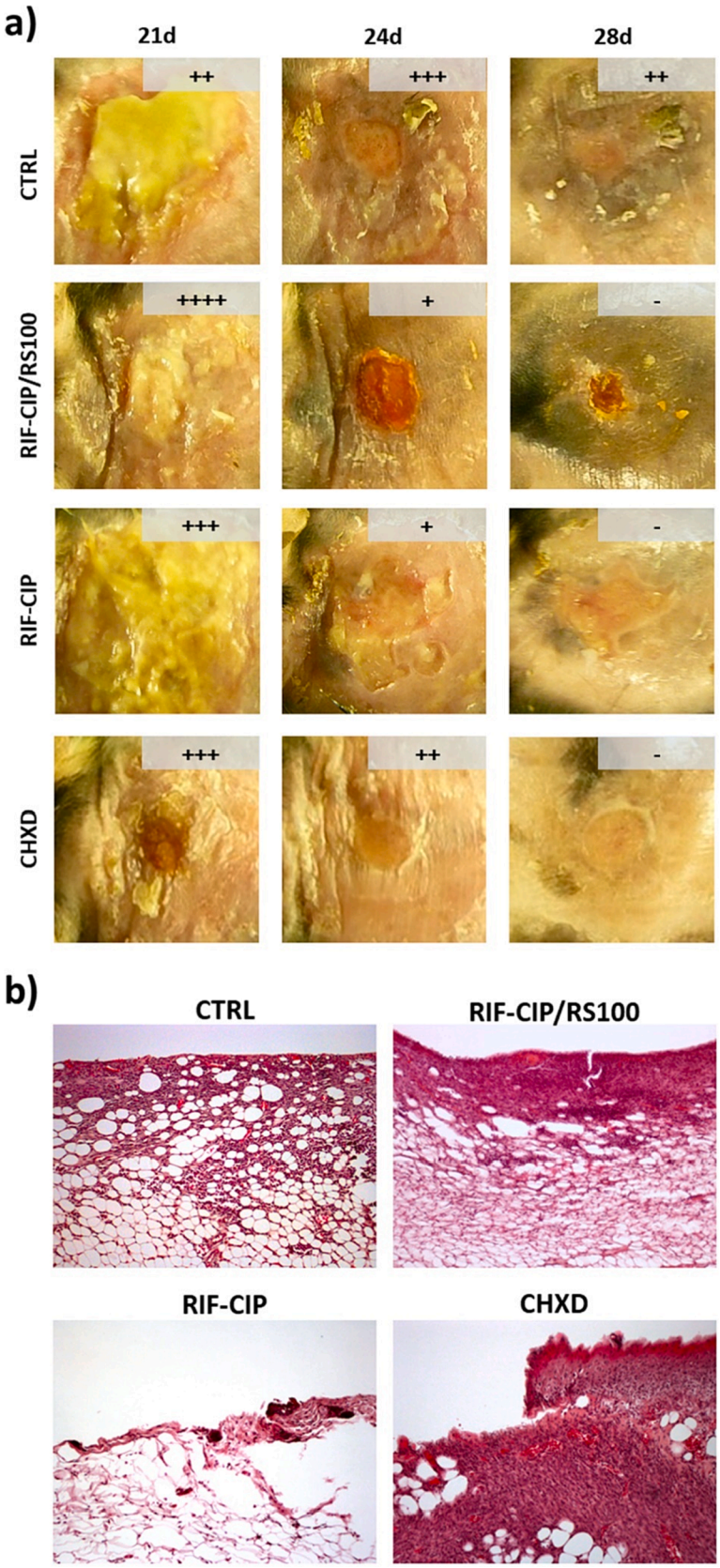

Fig. 6. *In vivo* evaluation of RIF-CIP/RS100 efficiency in a chronic infected murine model: a) Morphological and microbiological analyses of the wounds at different time points (21, 24 and 28 days PSI) in the experimental groups assayed (CTRL, RIF-CIP/RS100, free antibiotics (RIF-CIP), and the common antiseptic chlorhexidine (CHXD). Microbiological results in experimental and control groups are shown as insets. (-) no growth; (+) mild bacterial growth; (++) moderate bacterial growth; (+++) massive bacterial growth; (++++) extensive bacterial growth; b) Histopathological evaluation (HE; 10x) from the experimental groups analyzed. Representative images at 28 days PSI. The most intense fibrotic and inflammatory reaction is observed at the CHXD group. Hematoxylin-eosin x10.

non-healing wounds. In this regard, previous studies have also shown the *in vivo* efficiency of emulgels containing nanostructured lipid carriers with the antibiotic mupirocin though the bacterial challenge was much lower than ours (10^3 CFU/mL vs 10^7 CFU/mL) and wound healing was completely achieved after 15 days of treatment (daily 3 times per day) [56]. On the other hand, mupirocin was also used in the treatment of *S. aureus* Xen29 (10^9 CFU/mL) infected partial-thickness scald wound model in mice [57]. The treatment was administered twice per day during 7 days achieving the full wound closure at day 8. An infected (10^8 CFU in 500 μL by swabbing of MRSA) full-thickness scald wound model in rats was used to compare the potential healing of fusidic acid vs chlorhexidine among other compounds [58]. The animals were treated daily during 7 days showing that the antibiotic fusidic acid completely eradicated the bacterial load while the treatment with the antiseptic chlorhexidine significantly reduced the bacteria content in the scars though was not able to fully eliminate it. It is important to notice that in those *in vivo* studies mice and rats were not diabetic while in our work diabetic obese mice were used.

4. Conclusions

Electrospun Eudragit®-based mats decorated with electrosprayed Eudragit®-based microparticles containing rifampicin and ciprofloxacin (RIF-CIP/RS100) respectively were fabricated for their potential application in the management of infected chronic wounds. Synergy between both antibiotics is here reported. The presence of both antibiotics in microfibers and microparticles provides the system with an initial antibiotic burst release and a sustained one over time. The resulting antibiotic-loaded mats are able to eradicate both *E. coli* and *S. aureus* in their sessile and biofilm-forming forms. The cationic nature of the dressing might be responsible for its superior antimicrobial action compared to the same antibiotics in their free form, corroborating the importance of the contact to elicit a strong antimicrobial action. RIF-CIP/RS100 was able to eliminate bacteria while harmless to a battery of different eukaryotic cell lines. The *in vitro* results were successfully corroborated in an *in vivo* chronic infected murine model highlighting the efficiency of RIF-CIP/RS100 in eradicating *S. aureus* infection and facilitating wound closure. Antibiotic topical therapy is not recommended on open wounds but as a second line treatment for only infected non-healing wounds the dual system here described could constitute a potential successful clinical solution. Long-term clearance efficacy of those antibiotic combinations should be carefully analyzed to avoid reciprocal suppression.

Funding statement

This research was funded by the Spanish Ministry of Science and Innovation (grant number PID2020-113987RB-I00). We also acknowledge the financial support of MCIN/AEIhttps://doi.org/10.13039/501100011033 and the NextGenerationEU/PRTR thanks to the project PDC2021-121405-I00. L.G.M−C. acknowledges the financial support from the Mexican Council of Science and Technology (CONACyT) through doctoral grant #710618. C.R. and M.P. acknowledge the support from Aragon regional government (Orden CUS/803/2021 and Orden CUS/581/2020, respectively), whereas G.L. from the FPI program (PRE2018-085769, Spanish Ministry of Science, Innovation and Universities). G.M. gratefully acknowledges the support from the Miguel Servet Program (MS19/00092; Instituto de Salud Carlos III). CIBER-BBN is an initiative funded by the VI National R&D&i Plan 2008—2011, Iniciativa Ingenio 2010, Consolider Program, CIBER Actions and financed by the Instituto de Salud Carlos III (Spain) with assistance from the European Regional Development Fund.

Ethics approval statement

In vivo experiments were carried out in compliance with the Spanish Policy for Animal Protection RD53/2013 which meets the European Union Directive 2010/63, and under Project License PI59/22 approved by the Ethics Committee for Animal Experiments of the University of Zaragoza (Spain).

Patient consent statement

N/A

Permission to reproduce material from other sources

N/A

Clinical trial registration

N/A

Declaration of Competing Interest

The authors declare that they have no known competing financial interests or personal relationships that could have appeared to influence the work reported in this paper.

Data availability

Data will be made available on request.

Acknowledgements

This research was funded by the Spanish Ministry of Science and Innovation (grant number PID2020-113987RB-I00). We also acknowledge the financial support of MCIN/AEI/10.13039/501100011033 and the NextGenerationEU/PRTR thanks to the project PDC2021-121405-I00. L.G.M-C. acknowledges the financial support from the Mexican Council of Science and Technology (CONACyT) through doctoral grant #710618. C.R. and M.P. acknowledge the support from Aragon regional government (Orden CUS/803/2021 and Orden CUS/581/2020, respectively), whereas G.L. from the FPI program (PRE2018-085769, Spanish Ministry of Science, Innovation and Universities). G.M. gratefully acknowledges the support from the Miguel Servet Program (MS19/00092; Instituto de Salud Carlos III). CIBER-BBN is an initiative funded by the VI National R&D&i Plan 2008 -2011, Iniciativa Ingenio 2010, Consolider Program, CIBER Actions and financed by the Instituto de Salud Carlos III (Spain) with assistance from the European Regional Development Fund. We also thank the LMA-ELECMI ICTS (University of Zaragoza, Spain), the Cell Culture, Animal, and Pathological Anatomy Core Units from IACS/IIS Aragon for their instruments and expertise. We would like to thank Ander Cabrerizo for his helpful support.

References

[1] L.S. Altoé, R.S. Alves, M.M. Sarandy, M. Morais-Santos, R.D. Novaes, R. V. Gonçalves, Does antibiotic use accelerate or retard cutaneous repair? a systematic review in animal models, PLoS One 14 (10) (2019) e0223511, https://doi.org/10.1371/journal.pone.0223511.

[2] A.R. Unnithan, N.A.M. Barakat, P.B. Tirupathi Pichiah, G. Gnanasekaran, R. Nirmala, Y.-S. Cha, C.-H. Jung, M. El-Newehy, H.Y. Kim, Wound-dressing materials with antibacterial activity from electrospun polyurethane–dextran nanofiber mats containing ciprofloxacin HCl, Carbohydr. Polym. 90 (4) (2012) 1786–1793, https://doi.org/10.1016/j.carbpol.2012.07.071.

[3] P. Das Ghatak, S.S. Mathew-Steiner, P. Pandey, S. Roy, C.K. Sen, A surfactant polymer dressing potentiates antimicrobial efficacy in biofilm disruption, Sci. Rep. 8 (1) (2018) 873.

[4] N.T. Thet, J. Mercer-Chalmers, R.J. Greenwood, A.E.R. Young, K. Coy, S. Booth, A. Sack, A.T.A. Jenkins, SPaCE Swab: point-of-care sensor for simple and rapid detection of acute wound infection, ACS Sensors 5 (8) (2020) 2652–2657, https://doi.org/10.1021/acssensors.0c01265.

[5] A.L. Waterbrook, K. Hiller, D.P. Hays, M. Berkman, Do topical antibiotics help prevent infection in minor traumatic uncomplicated soft tissue wounds? Ann. Emerg. Med. 61 (1) (2013) 86–88, https://doi.org/10.1016/j.annemergmed.2012.08.002.

[6] C.F. Heal, J.L. Banks, P. Lepper, E. Kontopantelis, M.L. van Driel, Meta-analysis of randomized and quasi-randomized clinical trials of topical antibiotics after primary closure for the prevention of surgical-site infection, Br. J. Surg. 104 (9) (2017) 1123–1130, https://doi.org/10.1002/bjs.10588.

[7] C.D. Roberts, D.J. Leaper, O. Assadian, The role of topical antiseptic agents within antimicrobial stewardship strategies for prevention and treatment of surgical site and chronic open wound infection, Adv Wound Care (new Rochelle) 6 (2) (2016) 63–71, https://doi.org/10.1089/wound.2016.0701.

[8] D. Vucic, K. Cvitkusic-Lukenda, I. Dunder, K. Gabaldo, M. Knezevic-Pravecek, B. Miskic, Diagnostic complexity of rifampicin-induced coagulopathy in a patient

with spontaneous muscle bleeding A case report, Medicine 100 (26) (2021), https://doi.org/10.1097/md.0000000000026234.
[9] M.C. García, A.A. Aldana, L.I. Tártara, F. Alovero, M.C. Strumia, R.H. Manzo, M. Martinelli, A.F. Jimenez-Kairuz, Bioadhesive and biocompatible films as wound dressing materials based on a novel dendronized chitosan loaded with ciprofloxacin, Carbohydr. Polym. 175 (2017) 75–86, https://doi.org/10.1016/j.carbpol.2017.07.053.
[10] Y.R. Kang, D.R. Chung, J. Kim, J.Y. Baek, S.H. Kim, Y.E. Ha, C.I. Kang, K.R. Peck, J. H. Song, In vitro synergistic effects of various combinations of vancomycin and non-beta-lactams against Staphylococcus aureus with reduced susceptibility to vancomycin, Diagn. Microbiol. Infect. Dis. 86 (3) (2016) 293–299, https://doi.org/10.1016/j.diagmicrobio.2016.08.009.
[11] C.J. Coe, S.A. Doss, G.S. Tillotson, S.G.B. Amyes, Interaction of sub-inhibitory concentrations of ciprofloxacin and rifampicin against staphylococcus-aureus, Int. J. Antimicrob. Agents 5 (2) (1995) 135–139, https://doi.org/10.1016/0924-8579(95)90674-l.
[12] D.P. Konig, J.M. Schierholz, U. Munnich, J. Rutt, Treatment of staphylococcal implant infection with rifampicin-ciprofloxacin in stable implants, Arch. Orthop. Trauma Surg. 121 (5) (2001) 297–299, https://doi.org/10.1007/s004020000242.
[13] S. Payab, N. Jafari-Aghdam, M. Barzegar-Jalali, G. Mohammadi, F. Lotfipour, T. Gholikhani, K. Adibkia, Preparation and physicochemical characterization of the azithromycin-Eudragit RS100 nanobeads and nanofibers using electrospinning method, J. Drug Delivery Sci. Technol. 24 (6) (2014) 585–590, https://doi.org/10.1016/s1773-2247(14)50123-2.
[14] J. Chen, F.K. Xu, Y.D. Wei, J.W. Qi, Dual-carrier drug-loaded composite membrane dressings of mesoporous silica and layered double hydroxides, J. Drug Delivery Sci. Technol. 75 (2022), https://doi.org/10.1016/j.jddst.2022.103634.
[15] R. Ramalingam, C. Dhand, V. Mayandi, C.M. Leung, H. Ezhilarasu, S. K. Karuppannan, P. Prasannan, S.T. Ong, N. Sunderasan, I. Kaliappan, Core–shell structured antimicrobial nanofiber dressings containing herbal extract and antibiotics combination for the prevention of biofilms and promotion of cutaneous wound healing, ACS Appl. Mater. Interfaces 13 (21) (2021) 24356–24369.
[16] J. Chen, Z. Liu, M. Chen, H. Zhang, X. Li, Electrospun gelatin fibers with a multiple release of antibiotics accelerate dermal regeneration in infected deep burns, Macromol. Biosci. 16 (9) (2016) 1368–1380.
[17] S. Alizadeh, P. Farshi, N. Farahmandian, Z.A. Ahovan, A. Hashemi, M. Majidi, A. Azadbakht, M. Darestanifarahani, K.S. Sepehr, S.C. Kundu, Synergetic dual antibiotics-loaded chitosan/poly (vinyl alcohol) nanofibers with sustained antibacterial delivery for treatment of XDR bacteria-infected wounds, Int. J. Biol. Macromol. 229 (2023) 22–34.
[18] P. Sofokleous, E. Stride, M. Edirisinghe, Preparation, Characterization, and release of amoxicillin from electrospun fibrous wound dressing patches, Pharm. Res. 30 (7) (2013) 1926–1938, https://doi.org/10.1007/s11095-013-1035-2.
[19] M. Arruebo, V. Sebastian, Batch and microfluidic reactors in the synthesis of enteric drug carriers, Elsevier, Nanotechnology for Oral Drug Delivery, 2020, pp. 317–357.
[20] C. Lindholm, R. Searle, Wound management for the 21st century: combining effectiveness and efficiency, Int. Wound J. 13 (2016) 5–15.
[21] S. Jørgensen, R. Nygaard, J. Posnett, Meeting the challenges of wound care in Danish home care, J. Wound Care 22 (10) (2013) 540–545.
[22] J. Patel, F. Cockerill, P. Bradford, G. Eliopoulos, J. Hindler, S. Jenkins, S. Lewis, B. Limbago, A. Miller, D.P. Nicolau, M07–A10 methods for dilution antimicrobial susceptibility tests for bacteria that grow aerobically, Approved Standard 35 (2) (2015).
[23] L. Miranda-Calderon, C. Yus, G. Landa, G. Mendoza, M. Arruebo, S. Irusta, Pharmacokinetic control on the release of antimicrobial drugs from pH-responsive electrospun wound dressings, Int. J. Pharm. 624 (2022), 122003, https://doi.org/10.1016/j.ijpharm.2022.122003.
[24] R. Blakytny, E. Jude, The molecular biology of chronic wounds and delayed healing in diabetes, Diabet. Med. 23 (6) (2006) 594–608, https://doi.org/10.1111/j.1464-5491.2006.01773.x.
[25] S. Garcia-Salinas, E. Gamez, J. Asin, R. de Miguel, V. Andreu, M. Sancho-Albero, G. Mendoza, S. Irusta, M. Arruebo, Efficiency of antimicrobial electrospun thymol-loaded polycaprolactone mats in vivo, Acs Applied Bio Materials 3 (5) (2020) 3430–3439, https://doi.org/10.1021/acsabm.0c00419.
[26] D. Kathleen, J. Vandervoort, G. Van den Mooter, A. Ludwig, Evaluation of ciprofloxacin-loaded Eudragit((R)) RS100 or RL100/PLGA nanoparticles, Int. J. Pharm. 314 (1) (2006) 72–82, https://doi.org/10.1016/j.ijpharm.2006.01.041.
[27] B. Arauzo, M.P. Lobera, A. Monzon, J. Santamaria, Dry powder formulation for pulmonary infections: ciprofloxacin loaded in chitosan sub-micron particles generated by electrospray, Carbohydr. Polym. 273 (2021), https://doi.org/10.1016/j.carbpol.2021.118543.
[28] A. Dart, M. Bhave, P. Kingshott, Antimicrobial peptide-based electrospun fibers for wound healing applications, Macromol. Biosci. 19 (9) (2019), https://doi.org/10.1002/mabi.201800488.
[29] J.M. Deitzel, J. Kleinmeyer, D. Harris, N.C. Beck Tan, The effect of processing variables on the morphology of electrospun nanofibers and textiles, Polymer 42 (1) (2001) 261–272, https://doi.org/10.1016/S0032-3861(00)00250-0.
[30] S. Demirci, A. Celebioglu, Z. Aytac, T. Uyar, pH-responsive nanofibers with controlled drug release properties, Polym. Chem. 5 (6) (2014) 2050–2056, https://doi.org/10.1039/c3py01276j.
[31] T. Rongthong, S. Sungthongjeen, J. Siepmann, T. Pongjanyakul, Quaternary polymethacrylate-magnesium aluminum silicate films: Molecular interactions, mechanical properties and tackiness, Int. J. Pharm. 458 (1) (2013) 57–64, https://doi.org/10.1016/j.ijpharm.2013.10.016.
[32] S. Agrawal, R. Panchagnula, Implication of biopharmaceutics and pharmacokinetics of rifampicin in variable bioavailability from solid oral dosage forms, Biopharm. Drug Dispos. 26 (8) (2005) 321–334.
[33] M. Yasir, D. Dutta, M.D.P. Willcox, Enhancement of antibiofilm activity of ciprofloxacin against staphylococcus aureus by administration of antimicrobial peptides, Antibiotics-Basel 10 (10) (2021), https://doi.org/10.3390/antibiotics10101159.
[34] C. Yus, S. Irusta, V. Sebastian, M. Arruebo, Controlling particle size and release kinetics in the sustained delivery of oral antibiotics using pH-independent mucoadhesive polymers, Mol. Pharm. 17 (9) (2020) 3314–3327.
[35] M.M. Masadeh, K.H. Alzoubi, O.F. Khabour, S.I. Al-Azzam, Ciprofloxacin-induced antibacterial activity is attenuated by phosphodiesterase inhibitors, Current Therapeutic Research-Clinical and Experimental 77 (2015) 14–17, https://doi.org/10.1016/j.curtheres.2014.11.001.
[36] K.R. Baker, B. Jana, A.M. Hansen, H.M. Nielsen, H. Franzyk, L. Guardabassi, Repurposing azithromycin and rifampicin against gram-negative pathogens by combination with peptidomimetics, Front. Cell. Infect. Microbiol. 9 (2019) 236, https://doi.org/10.3389/fcimb.2019.00236.
[37] E.A. Rahal, N. Kazzi, A. Kanbar, A.M. Abdelnoor, G.M. Matar, Role of rifampicin in limiting Escherichia coli O157:H7 Shiga-like toxin expression and enhancement of survival of infected BALB/c mice, Int. J. Antimicrob. Agents 37 (2) (2011) 135–139, https://doi.org/10.1016/j.ijantimicag.2010.10.009.
[38] G. Aktas, S. Derbentli, In vitro activity of daptomycin combinations with rifampicin, gentamicin, fosfomycin and fusidic acid against MRSA strains, Journal of Global Antimicrobial Resistance 10 (2017) 223–227, https://doi.org/10.1016/j.jgar.2017.05.022.
[39] Y.S. Patel, S. Mehra, Synergistic response of rifampicin with hydroperoxides on mycobacterium: a mechanistic study, Front. Microbiol. 8 (2017), https://doi.org/10.3389/fmicb.2017.02075.
[40] S. Yang, X.M. Li, P. Liu, M.L. Zhang, C. Wang, B. Zhang, Multifunctional chitosan/polycaprolactone nanofiber scaffolds with varied dual-drug release for wound-healing applications, ACS Biomater Sci. Eng. 6 (8) (2020) 4666–4676, https://doi.org/10.1021/acsbiomaterials.0c00674.
[41] B.L. Wang, X. Chen, Z. Ahmad, J. Huang, M.W. Chang, Engineering on-demand magnetic core-shell composite wound dressing matrices via electrohydrodynamic micro-scale printing, Adv. Eng. Mater. 21 (10) (2019), https://doi.org/10.1002/adem.201900699.
[42] N.T. Thet, D.R. Alves, J.E. Bean, S. Booth, J. Nzakizwanayo, A.E.R. Young, B. V. Jones, A.T.A. Jenkins, Prototype development of the intelligent hydrogel wound dressing and its efficacy in the detection of model pathogenic wound biofilms, ACS Appl. Mater. Interfaces 8 (24) (2016) 14909–14919, https://doi.org/10.1021/acsami.5b07372.
[43] E.M. Hetrick, J.H. Shin, H.S. Paul, M.H. Schoenfisch, Anti-biofilm efficacy of nitric oxide-releasing silica nanoparticles, Biomaterials 30 (14) (2009) 2782–2789, https://doi.org/10.1016/j.biomaterials.2009.01.052.
[44] Y.S. Raval, A. Mohamed, L. Flurin, J.N. Mandrekar, K.E.G. Quaintance, H. Beyenal, R. Patel, Hydrogen-peroxide generating electrochemical bandage is active in vitro against mono- and dual-species biofilms, Biofilm 3 (2021), https://doi.org/10.1016/j.bioflm.2021.100055.
[45] S. Fulaz, H. Devlin, S. Vitale, L. Quinn, J.P. O'Gara, E. Casey, Tailoring nanoparticle-biofilm interactions to increase the efficacy of antimicrobial agents against staphylococcus aureus, Int. J. Nanomed. 15 (2020) 4779–4791, https://doi.org/10.2147/ijn.S256227.
[46] E. Gamez, G. Mendoza, S. Salido, M. Arruebo, S. Irusta, Antimicrobial electrospun polycaprolactone-based wound dressings: an in vitro study about the importance of the direct contact to elicit bactericidal activity, Adv Wound Care (new Rochelle) 8 (9) (2019) 438–451, https://doi.org/10.1089/wound.2018.0893.
[47] E.B. Kerekes, A. Vidács, M. Takó, T. Petkovits, C. Vágvölgyi, G. Horváth, V. L. Balázs, J. Krisch, Anti-biofilm effect of selected essential oils and main components on mono- and polymicrobic bacterial, Cultures 7 (9) (2019) 345.
[48] Z. Pandur, M. Dular, R. Kostanjsek, D. Stopar, Bacterial cell wall material properties determine E. coli resistance to sonolysis, Ultrason. Sonochem. 83 (2022), https://doi.org/10.1016/j.ultsonch.2022.105919.
[49] I. 10993-5:2009, Biological evaluation of medical devices — Part 5: Tests for in vitro cytotoxicity.
[50] C. Yus, R. Gracia, A. Larrea, V. Andreu, S. Irusta, V. Sebastian, G. Mendoza, M. Arruebo, Targeted release of probiotics from enteric microparticulated formulations, Polymers 11 (10) (2019) 1668.
[51] R. Lombardo, M. Ruponen, J. Rautio, C. Ghelardini, L. Di Cesare Mannelli, L. Calosi, D. Bani, R. Lampinen, K.M. Kanninen, A.M. Koivisto, E. Penttilä, H. Löppönen, R. Pignatello, Development of lyophilised eudragit® retard nanoparticles for the sustained release of clozapine via, Intranasal Administration 15 (5) (2023) 1554.
[52] J. Mattiazzi, M.H.M. Sari, R. Lautenchleger, M. Dal Prá, E. Braganhol, L. Cruz, Incorporation of 3,3'-diindolylmethane into nanocapsules improves its photostability, radical scavenging capacity, and cytotoxicity against glioma cells, AAPS PharmSciTech 20 (2) (2019) 49, https://doi.org/10.1208/s12249-018-1240-8.
[53] A.M. Mohyeldin, M.M. Mehanna, N.A. Elgindy, The relevancy of controlled nanocrystallization on rifampicin characteristics and cytotoxicity, Int. J. Nanomed. 11 (2016) 2209–2222, https://doi.org/10.2147/ijn.S94089.
[54] N. Ptaszyńska, K. Gucwa, K. Olkiewicz, M. Heldt, M. Serocki, A. Stupak, D. Martynow, D. Dębowski, A. Gitlin-Domagalska, J. Lica, A. Łęgowska, S. Milewski, K. Rolka, Conjugates of Ciprofloxacin and Levofloxacin with Cell-Penetrating Peptide Exhibit Antifungal Activity and Mammalian Cytotoxicity 21 (13) (2020) 4696.

[55] A. Gürbay, C. Garrel, M. Osman, M.J. Richard, A. Favier, F. Hincal, Cytotoxicity in ciprofloxacin-treated human fibroblast cells and protection by vitamin E, Hum. Exp. Toxicol. 21 (12) (2002) 635–641, https://doi.org/10.1191/0960327102ht305oa.

[56] P.V. Patil, M.D. Menon, A.D. Palshetkar, N.D. Desai, Topical delivery of mupirocin calcium nanostructured lipid carriers using a full-thickness excision wound healing model, J Wound Care 32(Sup5a) (2023) lxiii-lxxiv. https://doi.org/10.12968/jowc.2023.32.Sup5a.lxiii.

[57] A.D. Ogunniyi, Z. Kopecki, E.E. Hickey, M. Khazandi, E. Peel, K. Belov, A. Boileau, S. Garg, H. Venter, W.Y. Chan, P.B. Hill, S.W. Page, A.J. Cowin, D.J. Trott, Bioluminescent murine models of bacterial sepsis and scald wound infections for antimicrobial efficacy testing, PLoS One 13 (7) (2018), https://doi.org/10.1371/journal.pone.0200195.

[58] E. Ülkür, O. Oncul, H. Karagoz, E. Yeniz, B. Çeliköz, Comparison of silver-coated dressing (Acticoat™), chlorhexidine acetate 0.5% (Bactigrass®), and fusidic acid 2% (Fucidin®) for topical antibacterial effect in methicillin-resistant Staphylococci-contaminated, full-skin thickness rat burn wounds, Burns 31(7) (2005) 874-877. https://doi.org/https://doi.org/10.1016/j.burns.2005.05.002.